HHS Public Access

Author manuscript

Sens Actuators A Phys. Author manuscript; available in PMC 2017 November 01.

Published in final edited form as:

Sens Actuators A Phys. 2016 November 1; 251: 234–240. doi:10.1016/j.sna.2016.10.030.

An Angstrom-sensitive, differential MEMS capacitor for monitoring the milliliter dynamics of fluids

David J. Apigo[a], **Philip L. Bartholomew**[b], **Thomas Russell**[a], **Alokik Kanwal**[a], **Reginald C. Farrow**[a], and **Gordon A. Thomas**[a]

[a]New Jersey Institute of Technology, Department of Physics, Newark, NJ 07102, USA

[b]New Jersey Institute of Technology, Department of Material Science and Engineering, Newark, NJ 07201, USA

Abstract

A device, with MEMS sensors at its core, has been fabricated and tested for measuring low fluid pressure and slow flow rates. The motivation was to measure clinically relevant ranges of slow-moving fluids in living systems, such as the cerebrospinal fluid in the brain. For potential clinical utility, the device can be read transcutaneously by inductive coupling to MEMS capacitive sensors in circuits with resonance frequencies in the MHz range. Signal shifts for flow rates in the range of 0–42 mL/h and differential pressure levels between 0.1 and 2 kPa have been measured, because the sensitivity in the capacitance gap measurement is about 1 Å. The sensors have been used successfully to monitor simulated cerebrospinal fluid dynamics. The device does not utilize any internal power, since it is powered externally via the inductive coupling.

Keywords

bioMEMS; Slow fluid flow; Low pressure fluids; Shunt; Low pressure sensor; Flow sensor

1. Introduction

It was previously reported [1] that a capacitive type MEMS sensor can be utilized to measure the pressure and flow of the cerebrospinal fluid to determine functionality of a shunt that has been implanted to alleviate hydrocephalus. It is shown here that it is feasible to use a sensor of this type to measure the physiological parameters of cerebrospinal fluid (CSF) accurately in clinically relevant ranges. The reported sensors are formed by placing two chips against each other so that the recessed flexible membranes form a capacitor with a nominal spacing of approximately 1 μm. In both this case and the previously reported one, the shift in resonant frequency of an LC circuit is measured as the membrane spacing varies in response to pressure or flow rate. Differential capacitive sensors measure the pressure differential of CSF in a shunt flow path and are desirable for monitoring its dynamics because of their high sensitivity, low temperature sensitivity, and low power consumption

Correspondence to: David J. Apigo.

Supplementary data associated with this article can be found, in the online version, at http://dx.doi.org/10.1016/j.sna.2016.10.030.

[2]. While the motivation of this research was to monitor the dynamics of CSF, the MEMS sensor has the potential to be utilized in other applications as well as with other fluids (deionized water was used in the reported experiments). However, the majority of this paper will focus on the improvements made to the previously reported sensor and the results of tests that indicate higher sensitivity than previously reported.

1.1. Hydrocephalus and cerebrospinal fluid

Hydrocephalus is a condition in which proper flow of CSF is inhibited [3]. Most commonly, it is treated by diverting fluid flow with the implementation of a ventriculoperitoneal shunt that is inserted into a ventricle of the brain and drains into the peritoneal cavity, reducing the intracranial pressure (ICP) within the brain [3–5]. Each year, 39,000 shunt operations are performed, costing the health care industry over $1 billion [6]. If left untreated, the increased ICP can cause brain damage and eventual death [3]. The pressure is governed by the Monro-Kellie doctrine [7], which states that the sum of the volume of brain tissue, CSF, and cerebral blood remain constant. Therefore, if one of the three increases, the others must decrease to accommodate the change, possibly causing irreversible brain damage.

Commercial shunts are available for the treatment of hydrocephalus; however, their function is fairly limited. Simply stated, they are conduits equipped with a pressure sensitive valve that regulates the unidirectional flow of CSF [8]. Shunting has shown high success rates in correcting the flow of CSF in hydrocephalic patients [9]; however, they are not without flaw [6,10,11]. Malfunctioning shunts require patients to undergo invasive surgery to implant a new one, bringing about an increased risk of infection [12]. Currently, to determine if a revision is needed, physicians monitor patient symptoms, utilize advanced medical imaging, or perform invasive surgery to monitor the ICP of the individual [9,13]. A non-invasive method for monitoring the slow-flowing fluid dynamics is desired.

The physiological parameters of CSF are extremely difficult to monitor and cannot be observed with conventional sensors. In a healthy individual, the fluid is produced in the body at a rate of 0.35 mL/min (21 mL/h) [14,15] with pressure ranging between 2 and 18 mmHg [16–18]. For any fluid with parameters as small as these, one needs an extremely sensitive device; our estimates indicated that a capacitive sensor with sensitivity of 3.7 fF is required. This corresponds to a device capable of measuring 17 Pa (0.13 mmHg). This high sensitivity is required due to the nature of the fluid. Our results demonstrate that our sensor is 17 times more sensitive than needed. Typically sensors intended to measure this difficult-to-measure range of flow rates and pressures in various fluids can be broken down into one of three categories: optical [19], thermal [20,21], or MEMS [22–25]. Flow sensing has also been accomplished utilizing devices that measure the fluid's velocity via Doppler shift [26]. This paper will focus on two capacitive MEMS type sensors; one that is more sensitive towards pressure and another towards flow rate.

2. Theory of flexible membrane sensors

In order to measure said hydrodynamics, the sensors measure the differential pressure, ΔP, that exists as fluid flows through the tubing. The Hagen-Poiseuille equation describes the direct relationship between the fluid's volumetric flow rate, $\dot{V}$, and ΔP [24,27],

$$\Delta P = \dot{V}\ R_{hyd} \quad (1)$$

where R_{hyd} is the fluid's flow resistance, which can vary based on the geometry and length of the flow channel. In the current design, R_{hyd} is improved by a factor of 250 as previously reported [1]. This is accomplished in modifying the flow path by increasing the length of the flow path, L, between the flexible membranes from 1 mm to 25 cm. This length can be altered if higher flow resistance is sought. Hydraulic flow resistance can be determined by the equation [28,29],

$$R_{hyd} = \frac{8\eta L}{\pi r^4} \quad (2)$$

where η is the fluid viscosity, and r is the radius of the channel, which is fixed at 0.8 mm because of a standard in commercial devices.

For the case of a membrane in contact with the fluid, and as pressure is applied, the distance between the membrane and the plate changes, resulting in a change in capacitance, C, via the equation [30,31],

$$C(w_0) = \varepsilon_0 \int_0^a \frac{dxdy}{d - w_0} \quad (3)$$

where ε_0 is the permittivity of free space, w_0 is the membrane center deflection, and d is the undeflected membrane spacing. Previously, an analytical model of this system was well demonstrated by Pan, et al., which also indicated that this change in capacitance can be directly related to the load pressure [30].

Two sensors are utilized to acquire the change in pressure throughout the system. In order to improve sensitivity and minimize a gravity effect, new sensors needed to be designed. A schematic cross-section that demonstrates the sensors' structure and operation can be seen in Fig. 1. A variable MEMS capacitor with flexible membranes is used in a resonant LC circuit. This allows the capacitance of the sensors to vary as pressure is applied to flexible membranes. The load pressure flexes the membranes and causes the spacing between the membranes to change (Fig. 1c). This produces a measurable shift in resonant frequency and can be used to calculate the flow rate and pressure due to the fluid throughout the system. The effect of gravity on the pressure on the double-membrane sensor has been minimized by having the water on the two sides of the flexible membranes separated by only 1 μm. Eq. (3) holds true if there is a rigid plate and only one membrane is free to flex. The reported design includes one single-membrane sensor, that behaves as such and is sensitive towards pressure. Eq. (1) shows that a ΔP is $\dot{V}$ required to monitor. In a single-membrane sensor, only one membrane can flex; therefore, a second pressure cannot be monitored throughout the system.

In the reported previous design [1] $\dot{V}$ was measured by utilizing two pressure sensors to monitor this ΔP so that $\dot{V}$ could be calculated. In order to eliminate the need of a second single-membrane capacitor in the system to monitor ΔP, a differential capacitor was designed that has two flexible membranes. This adds a second deflection term to the capacitance equation and can $\dot{V}$ be seen in Eq. (4) and allows the sensor to measure ΔP, and thus $\dot{V}$. Due to its differential nature, the double-membrane sensor is more sensitive towards flow rate.

The main features of this improved sensor are circular flexible membranes. The capacitance can then be derived from Eq. (3) by substituting the deflection term for a circular membrane. When two flexible membranes are present, this results in the equation,

$$C=2\pi\varepsilon_0\int_0^{\mathrm{a}}\frac{r}{d-\left[w_1-R_1+\sqrt{R_1^2-r^2}\right]+\left[w_2-R_2+\sqrt{R_2^2-r^2}\right]}dr \quad (4)$$

where r is the radius of the circular membrane, R is the radius of curvature of the deflected membrane, and w is the center deflection of a membrane (the second deflection term is not present if only one membrane can flex). The subscripts of 1 and 2 indicate each individual membrane. Previously, only one membrane could flex; however, with the improved design, one or both membranes are free to deflect. In order to increase the sensitivity of the device, $d \approx 1\mu m$. These devices can be incorporated in a resonant circuit and operated telemetrically to induce power and acquire data, thus requiring no internal battery. Equation (4) can be modified to calculate the capacitance for a single-membrane sensor and results in the equation,

$$C=2\pi\varepsilon_0\int_0^{\mathrm{a}}\frac{r}{d-\left[w_1-R_1+\sqrt{R_1^2-r^2}\right]}dr \quad (5)$$

As fluid passes the membranes, the center deflection between the membranes changes. In turn, the capacitance can vary. This produces a measurable shift in the resonant frequency of the device as it responds to the fluid. An external coil, with an inductance, L, is used to read the frequency, and it is related to the capacitance by the equation [32],

$$f=\frac{1}{2\pi\sqrt{LC}} \quad (6)$$

By measuring f, capacitance, and, in turn, membrane center deflection can be acquired. Once the center deflection, w, is calculated, the pressure can be acquired via the Eq. (7),

$$P=C_0\frac{Et^3w}{r^4\ (1-v^2)}+C_1\frac{\sigma_0 tw}{r^2}+C_2\frac{Etw^3}{a^4\ (1-v)}=P_0+P_1+P_2 \quad (7)$$

where (for a circular membrane with fixed supports), C_0 = 5.33 [33], C_1 = 4, C_2 = 2.67 [30], σ_0 is the membrane's initial stress (σ_0 = 169.5MPa), t is the membrane thickness, E is the Young's modulus (E = 600GPa), r is the radius of the membrane (r = 250 μm), and v is Poisson's ratio (ν = 0.25). The values given within parentheses are the parameters used for the reported sensors. Each value plays a significant role in the membrane center deflection. The values were constrained by both the maximum diameter of the flow path and the stress of the materials. Utilizing a 500 μm diameter flexible membrane allows for maximum deflection without the two membranes touching. In addition, the diameter keeps it smaller than the channel diameters and allows it to bend less than an 800 μm flexible membrane.

For the low flow rates and pressures being studied, an approximately linear relationship exists between said parameter and the shift in resonant frequency. Typically, an inverse relationship exists between the frequency and capacitance; however, since the relevant physiological parameters are so small, this trend is not observed (see Supplemental Fig. 1).

3. Materials and methods

3.1. Process flow & chip assembly

The sensors are fabricated utilizing state-of-the-art MEMS technology. The main feature of the chips are circular flexible membranes with a diameter, d = 500μm (see Fig. 2). This geometry minimizes stress on the edges of the membrane while maximizing the sensitivity of the device [34]. The thickness, t, of each membrane is 1 μm. Individual chips are fabricated and then carefully aligned and sandwiched together using a jig to make a differential capacitor with a spacing of ~1 μm. If two chips equipped with flexible membranes are sandwiched, a device that is more sensitive to flow is acquired and will be referred to as a double-membrane sensor. A single-membrane sensor has one fixed plate and one flexible membrane chip sandwiched together and is more sensitive towards pressure.

Devices are fabricated on 100 mm silicon wafers with 1 μm of thermally grown oxide on both sides. 20 nm Al2O3 are deposited on the top side of the wafer using atomic layer deposition (ALD). Next 500 nm of low stress silicon nitride is deposited using plasma enhanced chemical vapor deposition (PECVD). Followed by 20 nm of Al2O3 via ALD and 500 nm of silicon oxide (SiO2) via PECVD. Using photolithography and reactive ion etching (RIE) the pattern of the metal electrode is opened through the oxide layer, using the Al2O3 as a stop layer. 700 nm of Ti is deposited conformally using sputtering, which is than chemical mechanically polished (CMP) until the Ti is flush with the oxide layer. Next 20 nm of Al2O3 is deposited using ALD to protect the Ti. 500 nm of low stress silicon nitride is deposited using PECVD on top of the Al2O3 layer, which will help to define the capacitor gap. Windows are opening into the nitride using both photolithography and RIE, to expose the contact pad and the capacitor. The contact pads are capped with 250 nm gold, to aid with wire bonding, by using photolithography, e-beam evaporation, and lift off. Next the thermal

oxide on the back side of the wafer is patterned using photolithography and RIE. The patterned oxide is used as a mask to etch through the wafer using a Bosch etch. This step releases the membranes. The remaining oxide mask on the back of the wafer is etched away using RIE. Chips are finally diced out of the wafer, and the photoresist stripped in 1165 then cleaned in IPA. A schematic process flow can be seen in Fig. 3.

The capacitive sensors are assembled outside of the package by sandwiching two individual chips together (see Fig. 2d) by utilizing a precision alignment jig that allows the two capacitor plates to be opposite each other within 10%. As long as the sensor is aligned enough to function properly, perfect alignment is not critical. In fact, if misaligned drastically, the sensor may still function; however, the experimental sensitivity will be reduced. Changing the geometry of the membranes assists in this step as well, since alignment of the membranes is not as critical as the previous design. Once aligned, the chips are held together by 2 beads of epoxy and a 0.2 μH inductor is attached with silver conductive epoxy. The chips are heat treated so the inductor adheres.

Once assembled, the sensor is placed in a custom package designed for *in vitro* trials. It is capable of housing one single membrane sensor and one double membrane sensor. Fluid flows through 0.8 mm diameter channels and tubing throughout the package. Flow is eased when the fluid comes into contact with the membranes through a channel that allows the fluid to touch the sensor. In order to prevent liquid leakage, O-rings are utilized that create a seal between the Side B of the sensors and the flow channels. The fluid enters the system from the ventricular end and comes into contact with the flexible membranes of both sensors through the holes (if present) on Side B of the sensors. It flows out of the package through more tubing and is rerouted by a U-turn piece back to the package. The fluid flows past the backside of the single-membrane sensor and into another U-turn before continuing back to the package where it touches the double-membrane sensor again. The turning of the tubing allows an increase in length and a 250 times improved flow resistance. An image of the device, including U-turn pieces, can be seen in Fig. 4.

3.2. Experimental apparatus

An artificial CSF flow path was designed for our experimentation (Fig. 5), but could be modified for studies pertaining to other fluids easily. A syringe is utilized as a reservoir to simulate the ventricular cavity. Fluid is free to flow through the system as described above and drains into a Petrie dish at atmospheric pressure atop a digital scale. This end of the apparatus simulates the peritoneal cavity. By collecting the fluid at the end of the system, a measurement of flow rate can be acquired by measuring the mass of the fluid that accumulates over time.

Variable hydrostatic pressure, $P = \rho gh$, can also be studied utilizing the setup, with ρ = density of the fluid, $g = 9.8 \frac{m}{s^2}$, and h = the height of the fluid. The pressure can be held static throughout the course of a trial by setting the height of the water level and pinching off the peritoneal end of the system. P can be varied by adjusting the height of the water in the reservoir.

The data is collected remotely utilizing a custom handheld LC Meter that is hooked up to a PC by carefully aligning the coupling coil over the sensor coil. Data is transmitted to the computer by custom software that takes over 15 trials per physiological parameter over 2.5 to 5 min. Each trial consists of one resonant peak of 1000 data points. The data is processed via a custom Python code that averages these points, resulting in the data below. Each point is an average of over 15 trials. The high speed averaging of our sensor allows for improved sensitivity. If only one resonant peak was sought, the collection time drops to approximately 1 s.

4. Results and discussion

4.1. Double membrane sensor results

Experiments were performed *in vitro* over a large range of flow rates (as low as 4 mL/h and as high as 40 mL/h). Data in Fig. 6 correspond to flow rates from 30 mL/h to 42 mL/h. Due to the limitation in producible flow rates in our experimental setup, data spanning a larger range is difficult to acquire. Typically, a range of 10 mL/h is feasible. First, a control experiment was run where it was maintained at a constant value of $\dot{V} = 34$ mL/hr ± 1 mL/h (circular data points). As can be seen in Fig. 6, a linear relationship with zero slope exists for the control data and there is no statistically significant drift over a 42-min time interval. The standard deviation, σ, (displayed by the error bars) for frequency shift was 5 kHz. The 3σ fluctuation in the data in the earlier time periods for the control can potentially be explained by a temperature variation. Normal physiological parameters for body temperature range between 36 °C and 37 °C [35,36]. Within these conditions, small fluctuations are possible in the measured resonant frequencies, but should be minimal.

As the flow rate changes, a resonant frequency shift is measurable in the kHz range (Fig. 5). A linear relationship exists governed by the equation $\Delta f = 0.015\,\dot{V}$. The uncertainty in measuring each data point is 7 kHz, as indicated by the error bars. This indicates that this device can be utilized to monitored fluid dynamics whether flow is slow or fast.

The data suggests that the pressure and flow rate sensitivity of a double-membrane sensor is 1 Pa and 0.02 mL/hr, respectively. A high-speed averaging technique is utilized to minimize error in signal-to-noise throughout the experiment. The sensitivity for pressure is acquired from the standard deviation of the frequency shift. Using Δf, it is possible to calculate ΔC, and in turn the change in membrane center deflection, w. This value of Δw can be substituted into Equation (6) to calculate the ΔP sensitivity, which can be used with the known flow resistance to calculate the $\dot{V}$ sensitivity. The double-membrane sensor is sensitive towards both pressure and flow since the two parameters are intrinsically joined together, but is more sensitive towards flow rate due to its differential nature. This high sensitivity permits the sensor to be utilized in any situation where extremely small pressures and flow rates exist.

4.2. Single membrane sensor results

In Fig. 7, the circular data points (control) show the linear relationship with zero slope between time and a constant pressure of 1225 Pa, and corresponds only to the x-axis. The

experiment was then run in a pressure range of 122 Pa to 2000 Pa with shifts in the resonant frequency measurable in the kHz range in a comparable time interval. This data corresponds to both x-axes. A linear relationship exists between the applied pressure and the frequency shift (square data points) resulting in the a linear relationship governed by the equation, $\Delta f = 123.29P$, where Δf is the frequency shift and P is the applied pressure. The standard deviations in the frequency shift for control and variable data is 4 kHz and 11 kHz, respectively, and is demonstrated by the error bars.

By following the same calculations to find the sensitivity for the double-membrane sensor, the data in Fig. 7 suggests that the single-membrane sensor has a sensitivity towards pressure of 0.65 Pa. Thus, the single-membrane sensor is almost twice as sensitive as the double-membrane sensor. This can be explained by the elimination of the second flexible membrane. Since only one membrane can flex, any uncertainty in the measurement of the second pressure in the system is eliminated. Therefore, the sensitivity depends on the flexing of only one membrane, not two. This may seem almost contradictory towards the statement in Section 3.1 that the double-membrane sensor is more sensitive towards flow than the single-membrane sensor; however, since $\dot{V}$ the second membrane is eliminated, the single-membrane sensor cannot determine ΔP or

In order to calculate the precision in our device for the double-membrane sensor, we had to assume that both membranes flex approximately the same amount. This, of course, is not realistic; however, in order to simplify the integral for the double-membrane sensor to acquire an analytical solution, the assumption had to be made. In the single-membrane sensor, no such assumption is necessary since it is simpler to solve.

5. Conclusions

Both pressure and flow sensing MEMS devices have been successfully designed and tested demonstrating that it is possible to monitor both parameters non-invasively in a hydrocephalic patient or other slow moving fluid. *In vitro* testing shows that it is possible to monitor flow rates over a range of 0 mL/h to 40 mL/hr, suggesting fluid flow can be studied over a range of slow flow rates. The devices demonstrate a measurable kHz range shift in the circuit's resonant frequency with a precision of ±7 kHz. Pressures between 0.1 and 2 kPa can be monitored with a single-membrane sensor with precision of ±11 kHz. Control studies of both sensors indicated a precision of approximately ±5 kHz. We have tested the single-membrane sensor and shown that it does not measure flow rate when pressure is constant. Also, without the use of a second single-membrane sensor, this sensor cannot monitor flow rate since no ΔP is measured. However, we have shown that under variable flow rate conditions, the double-membrane sensor is capable of monitoring both parameters.

The slopes for the flow rate versus shift in resonant frequency demonstrates a 17% error between the theoretical and experimental values. Theory predicts that the slope should be 0.018 (kHz·hr)/mL, while the experimental data shows it is actually 0.015 (kHz·hr)/mL. This difference can be explained by the uncertainty that exists in the unelected membrane spacing. The sensors were designed to have an undeflected spacing of 1 μm, but it is extremely difficult to be certain that is the exact spacing. Whatever uncertainty exists in the

membrane spacing is reflected in the absolute value of the slope between the flow rate and shift in frequency. Despite the uncertainty in the membrane spacing, the device behaves as expected, and will do so, unless the membranes touch.

Due to their ultra-sensitivity, the dynamics of CSF and other slow-flowing fluids can be monitored. The single-membrane sensor has a pressure precision of 0.65 Pa, while the double-membrane sensor has pressure and flow rate precisions of 1 Pa and 0.02 mL/hr, respectively. This opens the possibility of studying the fluid as it flows through shunt tubing. Monitoring proper shunt function is a consequence of such an ultra-sensitive device and future studies could examine the effects different drug therapies have on CSF dynamics in patients equipped with a shunt. Varying the membrane spacing could improve upon the sensitivity, if desired. To our knowledge, these are the most sensitive pressure and flow sensors.

In addition to monitoring the dynamics of CSF, this type of ultra-sensitive MEMS sensor can be utilized in other ways. They could prove useful in fields interested in difficult to measure pressures and flow rates, such as microfluidics. Since our sensor has a sensitivity in membrane center deflection of 1 Å, it should be possible to place atoms on our membrane and observe the deflection, and in turn be able to tell the mass of an atom. In a thorough review, Tsouti, et al., describe capacitive type MEMS sensors utilized in detecting specific molecules on the membrane surfaces by observing the stress interactions with the membrane [31]. Since this research focused on the dynamics of a particular fluid, further research is needed to examine how this device can be applied to other fields of study.

Supplementary Material

Refer to Web version on PubMed Central for supplementary material.

Acknowledgments

Funding

The National Institutes of Health (NINDS) supported this work and was performed under grant R43NS056628-01A2.

This work was performed in part at the Cornell NanoScale Facility, a member of the National Nanotechnology Coordinated Infrastructure (NNCI), which is supported by the National Science Foundation (Grant ECCS-1542081).

References

1. Raj R, Lakshmanan S, Apigo D, Kanwal A, Liu S, Russell T, et al. Demonstration that a new flow sensor can operate in the clinical range for cerebrospinal fluid flow. Sensor Actuat A: Phys. 2015; 234:223–231.
2. Chavan AV, Wise KD. Batch-processed vacuum-sealed capacitive pressure sensors, Microelectromechanical Systems. J Microelectromech Syst. 2001; 10:580–588.
3. Lee P, DiPatri AJ Jr. Evaluation of suspected cerebrospinal fluid shunt complications in children. Clin Pediatr Emerg Med. 2008; 9:76–82.
4. Robertson JS, Maraqa M, Jennett B. Ventriculoperitoneal shunting for hydrocephalus. Br Med J. 1973; 2:289. [PubMed: 4574347]

5. Ames RH. Ventriculo-peritoneal shunts in the management of hydrocephalus. J Neurosurg. 1967; 27:525. [PubMed: 6065126]
6. Walker CT, Stone Jonathan J, Jacobson Maxwell, Phillips Valerie, Silberstein Howard J. Revision rate of pediatric ventriculoperitoneal shunts after 15 years: clinical article. J Neurosurg: Pediatr. 2013; 11:5.
7. Tully B, Ventikos Y. Cerebral water transport using multiple-network poroelastic theory: application to normal pressure hydrocephalus. J Fluid Mech. 2011; 667:188–215.
8. Xu H, Wang Z, Liu F, Tan G, Zhu H, Chen D. Programmable shunt valves for the treatment of hydrocephalus: a systematic review. Eur J Paediatr Neurol. 2013; 17:454–461. [PubMed: 23830575]
9. Gallia GL, Rigamonti D, Williams MA. The diagnosis and treatment of idiopathic normal pressure hydrocephalus. Nat Clin Pract Neurol. 2006; 2:375–381. [PubMed: 16932588]
10. Tuli S, Drake J, Lawless J, Wigg M, Lamberti-Pasculli M. Risk factors for repeated cerebrospinal shunt failures in pediatric patients with hydrocephalus. J Neurosurg. 2000; 92:31–38. [PubMed: 10616079]
11. Di Rocco C, Massimi L, Tamburrini G. Shunts vs endoscopic third ventriculostomy in infants: are there different types and/or rates of complications? Childs Nerv Syst. 2006; 22:1573–1589. [PubMed: 17053941]
12. Simon TD, Hall M, Riva-Cambrin J, Albert JE, Jeffries HE, Lafleur B, et al. Infection rates following initial cerebrospinal fluid shunt placement across pediatric hospitals in the United States. Clinical article. J Neurosurg Pediatr. 2009; 4:156–165. [PubMed: 19645551]
13. Arbour R. Intracranial hypertension monitoring and nursing assessment. Crit Care Nurse. 2004; 24
14. Kandel, Eric JHSR., Jessell, Thomas M. Principles of Neural Science. McGraw-Hill Health Professions Division; New York, NY: 2000.
15. Smillie A, Sobey I, Molnar Z. A hydroelastic model of hydrocephalus. J Fluid Mech. 2005; 539:417–443.
16. Irani, DN. Cerebrospinal Fluid in Clinical Practice. Elsevier Health Sciences; 2009.
17. Merritt HH, Fremont-Smith F. The cerebrospinal fluid. J Nerv Mental Dis. 1935; 81:720.
18. Ayer JB. Cerebrospinal fluid pressure from the clinical point of view. Arch Neurol Psychiatr. 1925; 14:440.
19. Berthold, JW., Thompson, LB. Fiber Optic Flow Sensor. Google Patents; 1990.
20. Meng E, Li P-Y, Tai Y-C. A biocompatible Parylene thermal flow sensing array. Sensor Actuat A: Phys. 2008; 144:18–28.
21. Kuo JT, Yu L, Meng E. Micromachined thermal flow sensors—A review. Micromachines. 2012; 3:550–573.
22. Clark TM, Malpas SC, McCormick D, Budgett DM, Heppner P. Implantable multi-Modal sensor to improve outcomes in hydrocephalus management. IEEE Sens J. 2015; 15:6027–6035.
23. Chen LY, Tee BC-K, Chortos AL, Schwartz G, Tse V, Lipomi DJ, et al. Continuous wireless pressure monitoring and mapping with ultra-small passive sensors for health monitoring and critical care. Nat Commun. 2014; 5
24. Oosterbroek R, Lammerink T, Berenschot J, Krijnen G, Elwenspoek M, Van dan Berg S. A micromachined pressure/flow-sensor. Sensor Actuat A: Phys. 1999; 77:167–177.
25. Oosterbroek, R., Lammerink, T., Berenschot, J., van der Berg, A., Elwenspoek, M. Designing, Realization and Characterization of a Novel Capacitive Pressure/flow Sensor. Transducers ’97, 1997 International Conference on Solid State Sensors and Actuators; Chicago. 1997.
26. Cannata JM, Chilipka T, Yang H-C, Han S, Ham SW, Rowe VL, et al. Development of a flexible implantable sensor for postoperative monitoring of blood flow. J Ultrasound Med. 2012; 31:1795–1802. [PubMed: 23091251]
27. Mortensen, NA., Okkels, F., Bruus, H. Reexamination of Hagen-Poiseuille Flow: Shape-dependence of the Hydraulic Resistance in Microchannels. 2004.
28. Granger, RA. Fluid Mechanics. Dover Publications; 1995.
29. Landau, LD., Lifshitz, EM. Fluid Mechanics. 2. Pergamon; 1987, 2016. CHAPTER II – VISCOUS FLUIDS; p. 44-94.

30. Pan, JY., Lin, P., Maseeh, F., Senturia, SD. Verification of FEM analysis of load-deflection methods for measuring mechanical properties of thin films. Solid-State Sensor and Actuator Workshop, 4th Technical Digest; IEEE; 1990. p. 70-73.
31. Tsouti V, Boutopoulos C, Zergioti I, Chatzandroulis S. Capacitive microsystems for biological sensing. Biosens Bioelectron. 2011; 27:1–11. [PubMed: 21752630]
32. Akar O, Akin T, Najafi K. A wireless batch sealed absolute capacitive pressure sensor. Sensor Actuat A: Phys. 2001; 95:29–38.
33. Timoshenko, SP., Woinowsky-Krieger, S. McGraw-hill. Theory of plates and shells. 1959.
34. Ko WH, Wang Q. Touch mode capacitive pressure sensors. Sensor Actuat A: Phys. 1999; 75:242–251.
35. Farrar, J., Hotez, P., Junghanss, T., Kang, G., Lalloo, D., White, NJ. Manson's Tropical Diseases. Elsevier Health Sciences; 2013.
36. Marx, J., Walls, RR. Hockberger Rosen's Emergency Medicine-concepts and Clinical Practice. Elsevier Health Sciences; 2013.

Biographies

David J. Apigo received his M.S. in Applied Physics from New Jeresy Institute of Technology in 2013 where he is currently pursuing his Ph.D. He obtained a B.A. in Physics and Classical Humanities from Rutgers University in 2009. His primary research interests include MEMS devices, biosensing, microfluidics, nanomaterials, and finite element analysis.

Philip L. Bartholomew completed his B.S. in Applied Mathematics at the New Jersey Institute of Technology in December of 2015. He is currently continuing his education at NJIT pursuing his Master's degree in Material Science and Engineering. His research interests include applying dynamical systems and chaos to better understand biological systems. His primary research has been involved in the fields of MEMS devices, microfluidics, implantable biomedical devices, and nanotube deposition dynamics.

Thomas Russell received his BS in Energy from Brown University, an MS in Mechanical Engineering from Stanford University and a PhD in Electrical Engineering from Brown University. He is the holder of four patents. His employment history includes Member of Technical Staff at Bell Laboratories, Manager of Test at Alcoa Eloectronic Packaging, VP of Technology at Voice-It Worldwide, Chief Controls Engineer at BOC Edwards, and VP of Engineering at Veritech. He is currently CTO of a startup company developing novel photovoltaic modules. Dr. Russell also provides electronics design and dcevelopment consulting services for medical, automotive, industrial, and consumer products.

Alokik Kanwal completed his Bachelor of Science in Electrical/Computer Engineering and Physics from Rutgers University in 2002. He received his Ph.D. in Materials Science from Rutgers University in 2008. He is currently an Assistant Research Professor in the Department of Physics at New Jersey Institute of Technology located in Newark, NJ. His research is in biophysics, energy, and their applications at the nanoscale. He leads the nanoscale and microscale fabrication of devices designed to study these areas.

Reginald C. Farrow is a Research Professor in Physics at NJIT. He obtained his Ph.D. in Physics from Steven's Institute of Technology in 1984. He obtained a B.S. in Physics from the University of Rochester and a Masters degree from Rutgers University. Dr. Farrow joined Bell Laboratories in 1976 and performed research in condensed matter physics, materials science, electron microscopy, and nanofabrication. In 2001 he joined Agere Systems where he coordinated activities between modeling, design, and manufacturing to

introduce new technology into the most advanced communications ICs. At NJIT, Dr. Farrow's research explores the interface between nanotechnology and biohpysics.

Gordon A. Thomas is a professor of physics at the New Jersey Institute of Technology, and is currently studying and developing devices to prevent blindness, treat brain injury, and save soldiers' lives. The American Physical Society has honored him as a Fellow of the Society, partly for his discovery of how a metal changes into an insulator. He received an Sc.B. from brown, a Ph.D. from Rochester, and has conducted research at Tokyo, Harvard, the Massachusetts Institute of Technology, and Bell Laboratories. He has published about 150 papers and holds 15 patents in basic and applied physics.

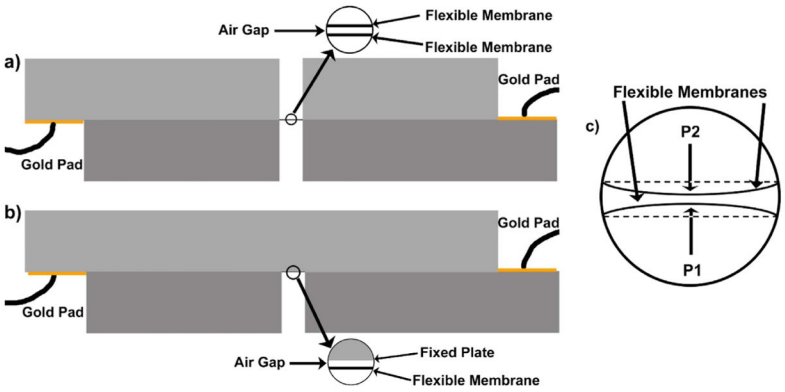

Fig. 1.

Schematic cross-section through the center of the hole in the silicon substrate surrounding the capacitor plates of a) a double-membrane sensor and b) a single-membrane sensor approximately to scale. Under no pressure, the Air Gap distance is ≤1 μm. c) Not-to-scale representation of when load pressures (P1 and P2) are exerted on the flexible membranes. The dotted line represents the undeflected membrane spacing. The air gap spacing varies due to a change in the membrane center deflection resulting in a change in capacitance, and a shift in the resonant frequency.

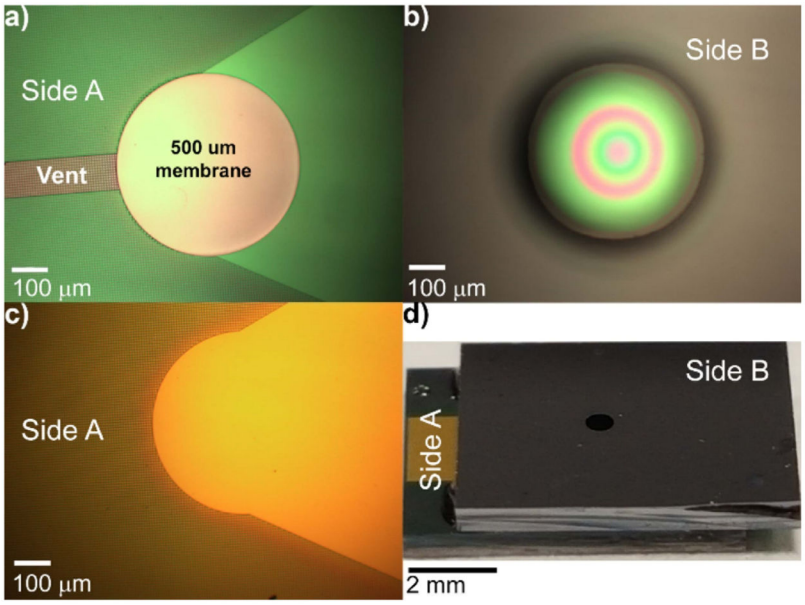

Fig. 2.

Images of sensor components. a) Microscope image of half a sensor focusing on its main feature, a 500 μm diameter circular flexible membrane. A 100 μm channel acts as a vent to allow trapped air to escape into a ballast within the package. b) Microscope image of the back of half of a sensor. If no flexible membrane is on Side A of the chip, the back is solid. c) Microscope image of a non-flexible plate. This allows the construction of a single-membrane sensor. d) Image of an assembled 5 mm × 6 mm sensor. Two chips are sandwiched together with Side A of each chip touching. Side B is exposed to the fluid. The square gold pad allows electrical connection to be made to and inductor to form an LC circuit.

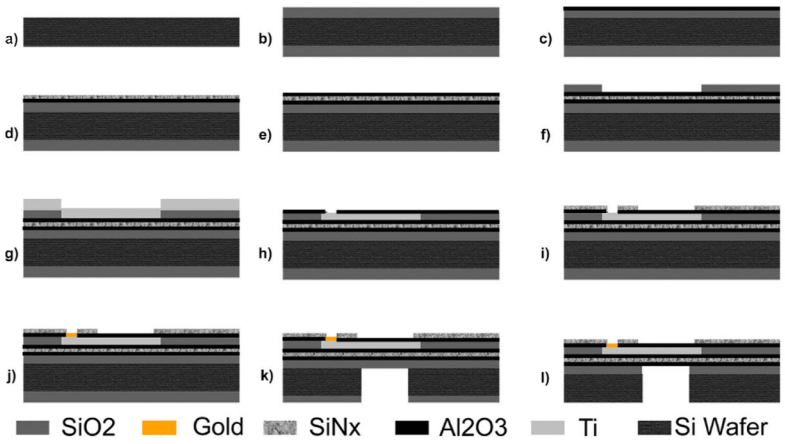

Fig. 3.

Schematic for process flow for fabricating chips used in the MEMS capacitor sensor. Steps follow “a” through “l”, see text for details.

Fig. 4.

Picture of chips housed within custom packaging. This design allows the fluid to pass all membranes that it touches in the same direction.

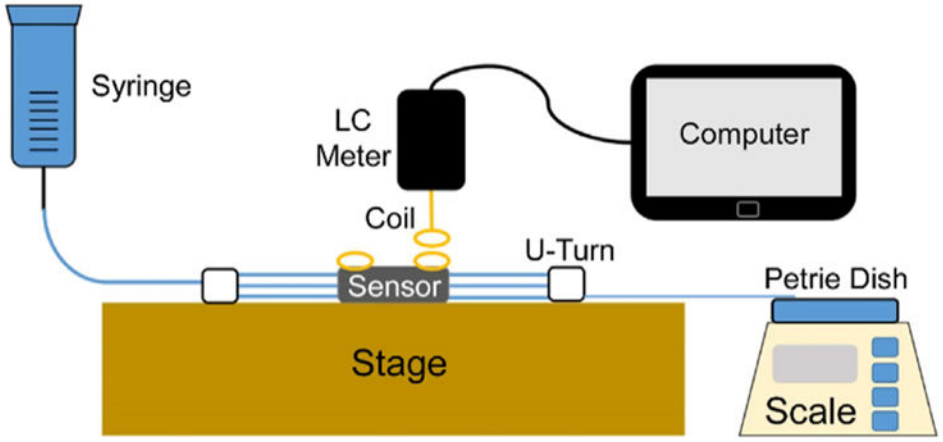

Fig. 5.

Schematic diagram of experimental artificial CSF flow path. The pressure difference in the system is driven by the volumetric flow rate in the tubing and the flow resistance. The circuit's resonant frequency can be read telemetrically by the LC meter.

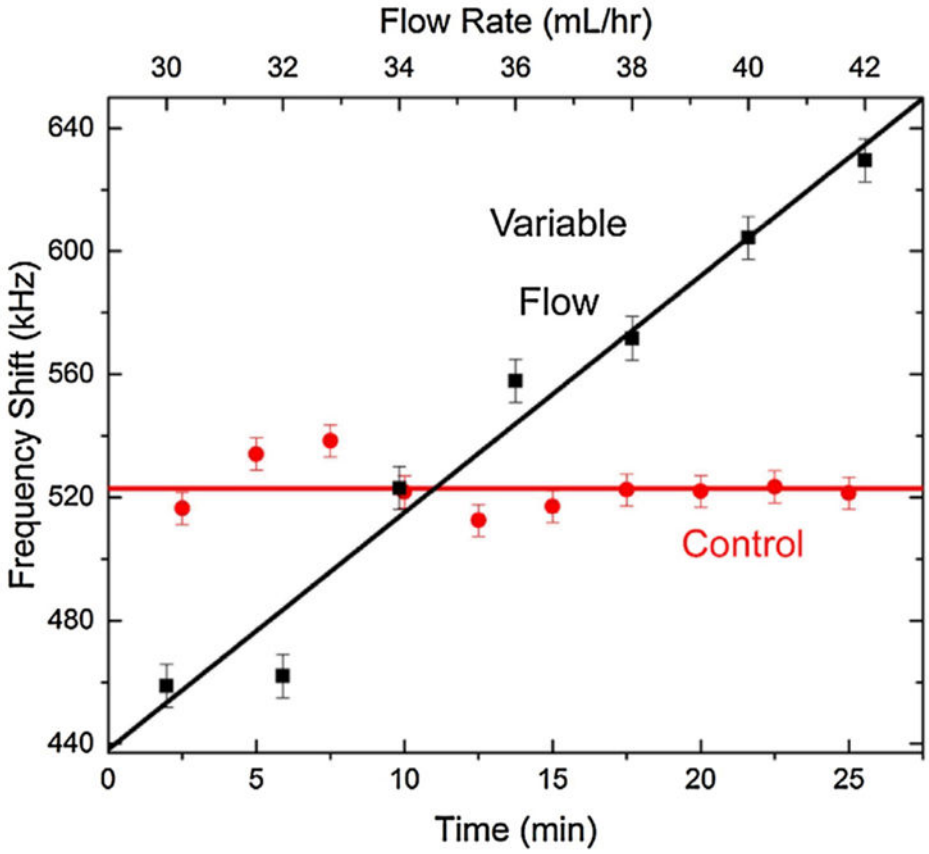

Fig. 6.

Double-membrane sensor evaluation tests. Control is at constant 34 mL/h and its corresponding pressure. Variable flow changes over time. Data showing the resonant frequency shift in a clinically relevant range for flow rate. Both control and variable flow data correspond to the lower x-axis, but the upper x-axis corresponds solely to the variable flow data.

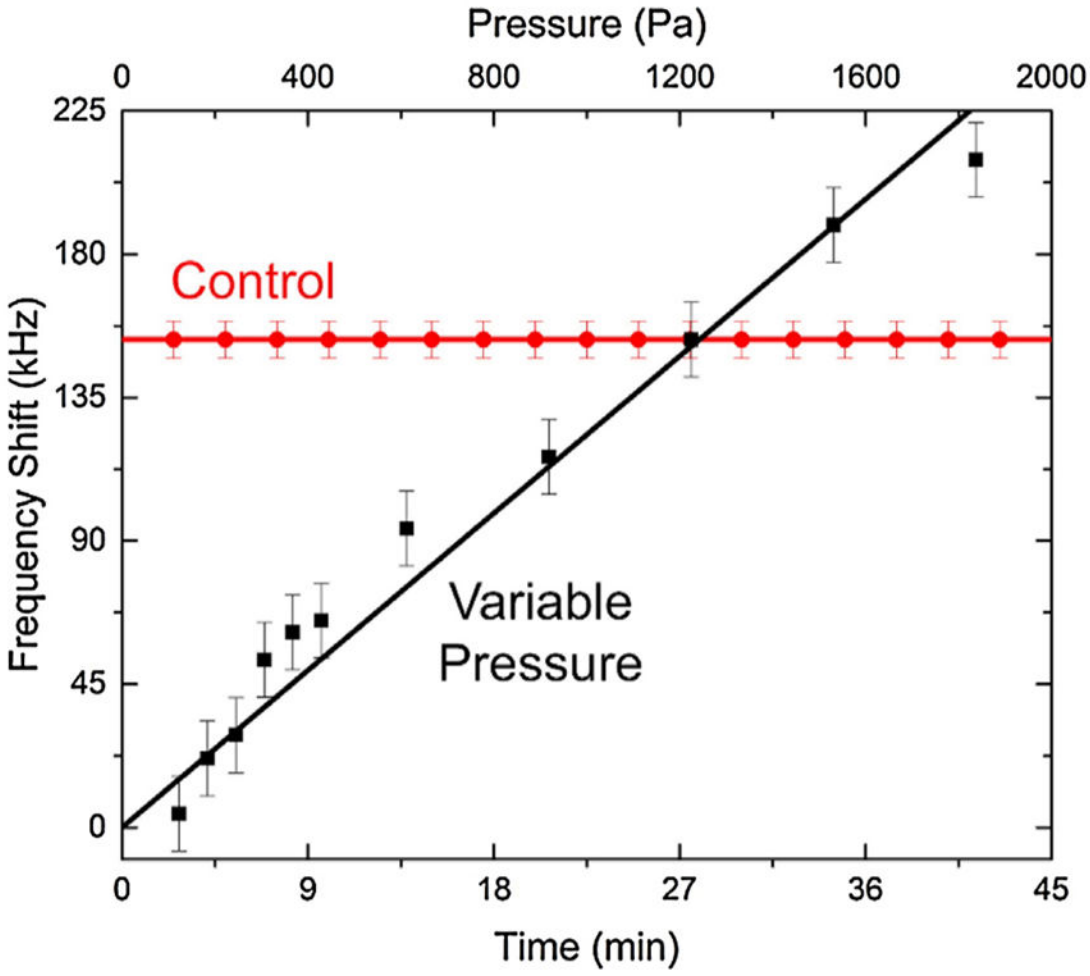

Fig. 7.

Single-membrane sensor evaluation test. Control kept at constant 1225 Pa and zero flow rate. Variable pressure changes over time. Data showing the resonant frequency shift in a clinically relevant range for pressure. Both control and variable pressure data correspond to the lower x-axis, but the upper x-axis corresponds solely to the variable pressure data.